

Microscopic origin of diagonal stripe phases in doped nickelates

Marcin Raczkowski

*Marian Smoluchowski Institute of Physics, Jagellonian University, Reymonta 4, PL-30059 Kraków, Poland and
Laboratoire CRISMAT, UMR 6508 CNRS-ENSICAEN, 6,
Boulevard du Maréchal Juin, 14050 CAEN Cedex, France*

Raymond Frésard

*Laboratoire CRISMAT, UMR 6508 CNRS-ENSICAEN, 6,
Boulevard du Maréchal Juin, 14050 CAEN Cedex, France*

Andrzej M. Oleś

*Marian Smoluchowski Institute of Physics, Jagellonian University, Reymonta 4, PL-30059 Kraków, Poland
(Dated: February 6, 2008)*

We investigate the electron density distribution and the stability of stripe phases in the realistic two-band model with hopping elements between e_g orbitals at Ni sites on the square lattice, and compare these results with those obtained for the doubly degenerate Hubbard model with two equivalent orbitals and diagonal hopping. For both models we determine the stability regions of filled and half-filled stripe phases for increasing hole doping $x = 2 - n$ in the range of $x < 0.4$, using Hartree-Fock approximation for large clusters. In the parameter range relevant to the nickelates, we obtain the most stable diagonal stripe structures with filling of nearly one hole per atom, as observed experimentally. In contrast, for the doubly degenerate Hubbard model the most stable stripes are somewhat reminiscent of the cuprates, with half-filled atoms at the domain wall sites. This difference elucidates the crucial role of the off-diagonal e_g hopping terms for the stripe formation in $\text{La}_{2-x}\text{Sr}_x\text{NiO}_4$. The influence of crystal field is discussed as well.

PACS numbers: 75.30.Kz, 71.10.Fd, 75.10.Lp, 75.50.Ee

I. STRIPE PHASES IN NICKELATES

Stripe phases are one of the most exciting phenomena of modern condensed matter physics. They have been observed in a variety of systems, including nickelates,^{1,2,3,4,5,6,7,8} cuprates,^{9,10,11,12,13,14,15} and manganites.^{16,17,18} Among them, layered $\text{La}_{2-x}\text{Sr}_x\text{CuO}_4$ (LSCO), $\text{La}_{2-x-y}\text{Nd}_y\text{Sr}_x\text{CuO}_4$ (Nd-LSCO), $\text{La}_{2-x}\text{Sr}_x\text{NiO}_4$ (LSNO), and $\text{La}_2\text{NiO}_{4+\delta}$ (LNO) compounds play plausibly the most prominent role. However the similarity between them is superficial only, and the stripes in the cuprates differ from the stripes in the nickelates in many respects. For instance, they are dynamical in the former, and static in the latter. In addition, in Nd-LSCO^{9,10,11,12,13,14} and LSCO,¹⁵ one finds the so-called *half-filled stripes*, with the density of one doped hole per two atoms along the domain wall (DW). In contrast, it is clear from a variety of experiments that magnetic states within doped NiO_2 planes of the nickelates are *filled stripes* with density of one doped hole per one atom in a DW.^{1,2,3,4,5,6,7,8}

The question of filling is not the only difference between the nickelate and cuprate stripes, however. Neutron diffraction measurements performed on Nd-LSCO revealed that magnetic peaks are displaced from the antiferromagnetic (AF) maximum at $\mathbf{Q}_{\text{AF}} = \pi(1, 1)$ to the points $\mathbf{Q}_s = \pi(1 \pm 2\epsilon, 1)$ and $\mathbf{Q}_s = \pi(1, 1 \pm 2\epsilon)$ and the shift ϵ depends linearly on hole doping x for $x < 1/8$, while it is almost constant at higher doping. These values correspond to a superposition of *vertical* (01) and

horizontal (10) DWs. The essentially identical modulation and doping dependence of ϵ was observed in superconducting crystals of LSCO with $x > 0.05$. Conversely, experiments on LSNO established that spin order is characterized by the wave vectors $\mathbf{Q}_s = \pi(1 \pm \epsilon, 1 \pm \epsilon)$ with $\epsilon \simeq x$ for $x < 1/3$, corresponding to a constant charge of one hole/Ni ion along a *diagonal* DW, in agreement with the predictions made in the pioneering works by Zaanen and Gunnarsson¹⁹ and others,^{20,21,22,23} and emphasized recently,²⁴ which predicted theoretically the stripe order. More precisely, neutron scattering measurements have revealed static stripe order in the LNO samples with $\delta = 0.105, 0.125$, as well as 0.133 ,^{25,26,27,28,29,30,31} and even over a wider hole doping regime $0.135 \leq x \leq 0.5$ in the case of LSNO.^{1,2,3,4,5,6,7,8} Moreover, the incommensurate (IC) stripe order persists up to $x = 0.7$ in the $\text{Nd}_{2-x}\text{Sr}_x\text{NiO}_4$ system,³² in which the low temperature orthorhombic phase seems to extend to a higher doping region $x \leq 0.45$ as compared to the La compounds, where the high temperature tetragonal phase is stabilized instead already at $x \simeq 0.22$.¹

Indications of a charge order (CO) in doped LSNO were also found in electron³³ and x-ray diffraction studies.^{34,35,36} Quite recently, the one-dimensional nature of the stripe modulation within NiO_2 planes has been directly confirmed in the transmission electron microscopy (TEM) studies of charge stripes in LSNO.³⁷ In addition, careful examination of the TEM images has shown that at a low temperature stripes are mainly centered on rows of Ni atoms. However, a mixture of the so-

called site centered (SC) and bond centered (BC) stripes was also observed in some small regions of the sample. In contrast to LSCO, charge and spin order in LSNO is characterized by the wave vectors $\mathbf{Q}_c = 2\pi(\epsilon, \epsilon)$ and $\mathbf{Q}_s = \pi(1 \pm \epsilon, 1 \pm \epsilon)$, see Ref. 38, respectively, with $\epsilon \simeq x$ corresponding to a constant charge density of one hole/Ni ion along the diagonal stripe. Note that the doping dependence of ϵ is exactly the same as that found in the seminal Hartree-Fock (HF) calculations within the Hubbard model.^{19,20,21,22,23}

Experimentally the data give a clear evidence that the stripe order is most stable at hole doping $x = 1/3$. Indeed, $T_{\text{CO}}^{\text{IC}}$ and T_N increase linearly with x , reach a maximum at $x = 1/3$ with 240 and 180 K, respectively, and then decrease monotonously upon further doping. The particularly robust stability of stripes at $x = \epsilon = 1/3$ stems from the cooperative spin and charge modulation expressed by the coincidence of the spin superlattice peaks at the wave vectors $(1/2 \pm \epsilon/2, 1/2 \pm \epsilon/2)$ with those of CO, given by (ϵ, ϵ) . One should also note that ϵ starts to deviate gradually from the value given by the $\epsilon \simeq x$ law above $x = 1/3$. In fact, CO is even more stable than the stripe order at $x = 1/2$ and forms a checkerboard pattern below the transition temperature $T_{\text{CO}}^{\text{C}} \simeq 480$ K. Remarkably, with decreasing temperature, a stripe CO sets in below $T_{\text{CO}}^{\text{IC}} \simeq 180$ K and its incommensurability is twice as large as that of the spin order with the much lower onset temperature $T_N \simeq 80$ K.^{7,8} The low temperature competition of the checkerboard and stripe order at $x = 1/2$ has also been clearly indicated by the measurements of Raman and optical conductivity.^{39,40,41} Interestingly, above this doping, incommensurability tends to saturate rapidly with the value $\epsilon \simeq 0.44$.³²

Apparently, CO itself induces commensurate values of ϵ and such a commensurability effect seems to be an intrinsic property of the stripe order. At the same time, the increased hole density at the DWs suppresses the superexchange energy gain, best optimized when all the holes are accommodated within stripes. Therefore, it is the AF order that drives ϵ to approach the value given by the linear relation $\epsilon \simeq x$ below T_N . Obviously, when $x = 1/3$, both effects cooperate which results in the locked-in value of $\epsilon \simeq 1/3$ over the entire $T < T_{\text{CO}}^{\text{IC}}$ range.

Furthermore, the temperature dependence of the specific heat C_V shows a distinct anomaly at the same temperature $T_{\text{CO}}^{\text{IC}} = 240$ K suggesting a CO transition.⁴² This conjecture is supported by the temperature dependence of the logarithmic resistivity. Indeed, as expected for this transition, $\log \rho$ of the sample with $x = 0.3$ exhibits a steep increase precisely at 240 K.⁴³ Charge fluctuations around $T_{\text{CO}}^{\text{IC}} = 240$ K also lead to conspicuous changes in the optical conductivity spectra $\sigma(\omega)$.⁴⁴ Namely, at a high temperature $T > T_{\text{CO}}^{\text{IC}}$, only a broad peak is observed with a finite low-energy spectral weight. However, when T is decreased down to $T_{\text{CO}}^{\text{IC}}$, the low-energy weight below 0.4 eV is gradually transferred to higher energy so that the opening of the charge gap is clearly observed.

A special character of $x = 1/3$ as well as $x = 1/2$

doping, is best seen in the magnetic susceptibility χ and logarithmic resistivity $\log \rho$, recorded at 200 K, showing distinct anomalies at these doping levels.⁴³ In this context it is important to discuss a peculiar behavior of the Hall coefficient R_H and the Seebeck coefficient S at two representative values of temperature below and above $T_{\text{CO}}^{\text{IC}} = 240$ K, i.e., at 300 K and 210 K. The Hall coefficient at 300 K is almost independent of doping and takes a small positive value corresponding to the order of one hole carrier per Ni site.⁴⁵ The Seebeck coefficient shows a similar nearly constant behavior taking, however, a negative value. In contrast, below $T_{\text{CO}}^{\text{IC}}$, both R_H and S change their signs from negative to positive at $x = 1/3$ and their absolute values are larger than those at 300 K. In addition, for samples with $x = 0.3$ and 0.33, R_H keeps decreasing with decreasing T , so that the number of carriers per Ni site gets reduced even down to 0.01.

These results indicate that the deviation of x from $1/3$ can be considered as an electronlike ($x < 1/3$) or holelike ($x > 1/3$) carrier doping into the $\epsilon = 1/3$ charge-ordered insulator with three Ni sites in the unit cell. Hence, for the doping level $x = 1/3$ there is exactly one hole per unit cell and such a state is robust and may be considered as a half-filled one. Moreover, it would certainly retain this feature if the incommensurability had followed precisely the relation $\epsilon = x$. However, ϵ has a tendency to shift towards $1/3$, for both sides of the $x = 1/3$ point, which has important implications for the sign of R_H . On the one hand, when x is less than $1/3$, the number of holes is insufficient for filling up the mid-gap states entirely, i.e., the states inside the charge transfer (CT) gap induced by stripe order, and in this case the mid-gap states contain some electrons which become carriers. On the other hand, for x larger than $1/3$, the number of electrons is insufficient for filling up the lower Hubbard band entirely, which initially contains holes. Consequently, R_H is expected to have the opposite sign to that in the case of $x < 1/3$ (hole carriers).

Next, the chemical potential shift $\Delta\mu$ in LSNO for $x \leq 1/3$ deduced either from x-ray (XPS) or ultraviolet photoemission spectroscopy⁴⁶ is suppressed. Certainly, this phenomenon cannot be explained within a simple rigid-band framework in which μ is expected to shift downwards with increasing hole doping. In fact, an increase of x in a system with a spatially uniform hole distribution should enhance the average hole-hole repulsion which, in turn, would result in a higher energy required to add one hole to the system, i.e., in a larger $|\mu|$. Therefore, the absence of $\Delta\mu$ implies that the average hole-hole repulsion remains nearly unaltered upon doping. Such a behavior might be easily explained within a stripe picture in which a constant hole density at the DWs implies that the interwall distance decreases and ϵ increases linearly with increasing x . Moreover, a similar suppression of the shift has been found below $x \leq 1/8$ in LSCO, suggesting that an inhomogeneous charge distribution is a common feature of both systems.

Several methods have been employed to investigate the

stripe phases which go beyond the HF approximation, such as: density matrix renormalization group,^{47,48} slave-boson approximation,^{49,50,51} variational local ansatz approximation,⁵² exact diagonalization (ED) of finite clusters,⁵³ analytical approach based on variational trial wave functions within the string picture,^{54,55} dynamical mean field theory,⁵⁶ cluster perturbation theory,⁵⁷ and quantum Monte Carlo simulations.^{58,59} They all address the crucial role of a proper treatment of local electron correlations in stabilization of the half-filled stripe phases in the cuprates. In spite of this huge effort, it remains unclear whether DWs are centered on rows of metal atoms as in SC stripes, or if they are centered on rows of oxygen atoms bridging two metal sites in BC stripes.

Although no evidence was presented yet, it seems that the degeneracy of $3d$ orbitals plays an important role in stabilizing filled stripes in the nickelates. In the simplest picture developed for the cuprates, the Cu^{3+} ions forming DWs are spinless, while the Cu^{2+} of the AF domains carry a spin $S = 1/2$. In the nickelates, filled DWs are formed of the Ni^{3+} ions ($S = 1/2$), whereas the AF domains consist of Ni^{2+} ions ($S = 1$). Therefore, a realistic Hamiltonian for LSNO has to contain, besides the $x^2 - y^2$ orbital which is occupied by one hole in the parent compounds of the superconducting cuprates (such as La_2CuO_4 and $\text{YBa}_2\text{Cu}_3\text{O}_6$), as well the $3z^2 - r^2$ orbital at each ion, so as to account for the high spin ($S = 1$) state of the stoichiometric compound. Indeed, when extending their approach to a more realistic four-band Peierls-Hubbard model for NiO_2 planes, Zaanen and Littlewood have shown⁶⁰ that doped holes prone to form diagonal DWs, centered on rows of Ni atoms, with a tendency to have a ferromagnetic (FM) alignment of the reduced Ni magnetic moments at a DW. In fact, subsequent multiband HF calculations emphasized the relevance of the electron-lattice coupling — depending on its strength one can obtain either metal- or oxygen-centered structures.^{61,62} Therefore, it appears that the semiclassical theory captures the essence of stripe physics in the nickelates.

The stripes were also obtained in the theory using either the HF approximation applied to a multiband CT model, in which both the nickel and oxygen degrees of freedom are explicitly taken into account,^{60,61,62} or by the ED of finite clusters within the effective two-band model (1) extended by the coupling of e_g electrons to the lattice.⁶³ However, due to a large number of basis states, the latter calculation has solely been done for an eight site cluster allowing only for investigating stripe phases with a small unit cell observed experimentally at high doping levels $x = 1/3$ and $x = 1/2$. In contrast, the HF approximation used here allows one to describe charge and spin modulation with larger unit cells and hence it should provide an answer to the important question whether the description of NiO_2 planes by the simplified effective e_g model described below yields results consistent with the predictions of the CT model.^{60,61,62} An important aspect of these studies, qualitatively dif-

ferent from the pioneering work on the cuprates where the relevant models yield DWs with *nonmagnetic* Cu^{3+} ions,^{19,20,21,22,23} is that DWs in the nickelates are formed of Ni^{3+} ions carrying a *finite* spin $S = 1/2$ leading to a FM polarization around them.

In this work we investigate various stripe phases resulting from an effective Hamiltonian for e_g electrons relevant to the NiO_2 layers, and compare them with those obtained in the doubly degenerate Hubbard (DDH) model. We use the HF approximation in order to gain the qualitative insight into possible stripe phases and their stability. This approach is the first step to make in order to identify possible generic instabilities towards stripe phases in NiO_2 planes, in analogy to the early work on CuO_2 planes which predicted the existence of stripes in the high T_c cuprates.¹⁹ The HF method is well suited to compare the energies of different types of magnetically ordered phases, as it approaches the same limit at $U \rightarrow \infty$ as better mean-field theories, such as slave-boson approach or the Gutzwiller ansatz.⁶⁴ In addition, the HF approach allows one for efficient calculations on large clusters at low temperatures which are necessary to obtain unbiased results concerning the stability of various stripe phases, particularly when the magnetic (and charge) unit cells are large at low doping.

The paper is organized as follows. The models with orbital degeneracy are introduced in Sec. II. The energy of various stripe phases, filled vs. half-filled, diagonal vs. vertical, together with the influence of the various parameters of the model, are presented in Sec. III. Their structures are further described in Sec. IV, together with the mechanism which leads to their stability, illustrated by the double occupancy distribution and by the respective densities of states. The paper is summarized in Sec. V, where we also present our main conclusions.

II. TWO-BAND HUBBARD MODELS

Even though doped nickelate LSNO is isostructural to its cuprate counterpart LSCO, the electronic degrees of freedom in LSNO are more involved. In fact, a minimal realistic Hamiltonian for LSNO must contain, besides the $x^2 - y^2$ orbital states included in the cuprate oxide models, also the $3z^2 - r^2$ orbital states. Such a model of interacting e_g electrons in a 2D (a, b) plane may be written as follows,

$$\mathcal{H} = H_{\text{kin}} + H_{\text{int}} + H_z, \quad (1)$$

with two orbital flavors, $|x\rangle \equiv x^2 - y^2$ and $|z\rangle \equiv 3z^2 - r^2$, forming a basis in the orbital space. The kinetic energy is described by

$$H_{\text{kin}} = \sum_{\langle ij \rangle} \sum_{\alpha\beta\sigma} t_{\alpha\beta} c_{i\alpha\sigma}^\dagger c_{j\beta\sigma}, \quad (2)$$

with

$$t_{\alpha\beta} = -\frac{t}{4} \begin{pmatrix} 3 & \pm\sqrt{3} \\ \pm\sqrt{3} & 1 \end{pmatrix}, \quad (3)$$

where t stands for an effective ($dd\sigma$) hopping matrix element due to the hybridization with oxygen orbitals on Ni–O–Ni bonds, and the off-diagonal hopping t_{ij}^{xz} along a and b axis depends on the phase of the $|x\rangle$ orbital along the considered cubic direction. The electron-electron interactions contain only on-site terms, which we write in the following form,

$$H_{\text{int}} = U \sum_i (n_{ix\uparrow}n_{ix\downarrow} + n_{iz\uparrow}n_{iz\downarrow}) + (U - \frac{5}{2}J_H) \sum_i n_{ix}n_{iz} - 2J_H \sum_i \mathbf{S}_{ix} \cdot \mathbf{S}_{iz} + J_H \sum_i (c_{ix\uparrow}^\dagger c_{ix\downarrow}^\dagger c_{iz\downarrow} c_{iz\uparrow} + c_{iz\uparrow}^\dagger c_{iz\downarrow}^\dagger c_{ix\downarrow} c_{ix\uparrow}), \quad (4)$$

where U and J_H stand for the intraorbital Coulomb and Hund's exchange elements. We also used $n_{i\alpha} = \sum_\sigma n_{i\alpha\sigma}$ for total electron density operators, given by the sum of densities in orbitals $\alpha = x, z$. The last term H_z describes the uniform crystal-field splitting between $|x\rangle$ and $|z\rangle$ orbitals along the c axis,

$$H_z = \frac{1}{2}E_z \sum_{i\sigma} (n_{ix\sigma} - n_{iz\sigma}). \quad (5)$$

The splitting between the e_g orbitals originates from the tetragonal Jahn-Teller distortion of the NiO_6 octahedron. In La_2NiO_4 , however, the octahedron where the Ni–O–Ni in-plane (out-of-plane) bond lengths are 1.95 (2.26) Å,⁶⁵ respectively, is much less distorted as compared to 1.89 and 2.43 Å bonds in La_2CuO_4 ,⁶⁶ which reflects the difference in electron filling. In what follows we consider only a realistic positive E_z favoring, due to elongated octahedra, the $|z\rangle$ electron occupancy over the $|x\rangle$ occupancy in doped compounds.

In order to elucidate the mechanism leading to the stabilization of the stripes, we also investigate the DDH model. It is obtained using the hopping matrix,

$$t_{\alpha\beta} = -\frac{t}{2} \begin{pmatrix} 1 & 0 \\ 0 & 1 \end{pmatrix}, \quad (6)$$

instead of Eq. (3). Note, that the total bandwidth is $W = 6t$ in the e_g model and $W = 4t$ in the DDH model (at $E_z = 0$), but the average diagonal hopping elements are the same — this ensures that electrons are approximately similarly correlated for a given U in both cases, while the electron-electron interactions have in the DDH model the same form given by Eq. (4), provided one labels the orbitals as x and z .

The model given by Eq. (1) is very rich. Even when restricting oneself to solutions with only two atoms in the unit cell, one obtains an intricate competition between numerous FM and AF phases, even on the level of mean field (MF) approximation.⁶⁷ In particular, we obtained phase diagrams showing, in the regime away from half filling, a clear tendency towards ferromagnetism for $J_H \simeq U/4$, or at least to the C -AF phase for $J_H \simeq 0.15U$.

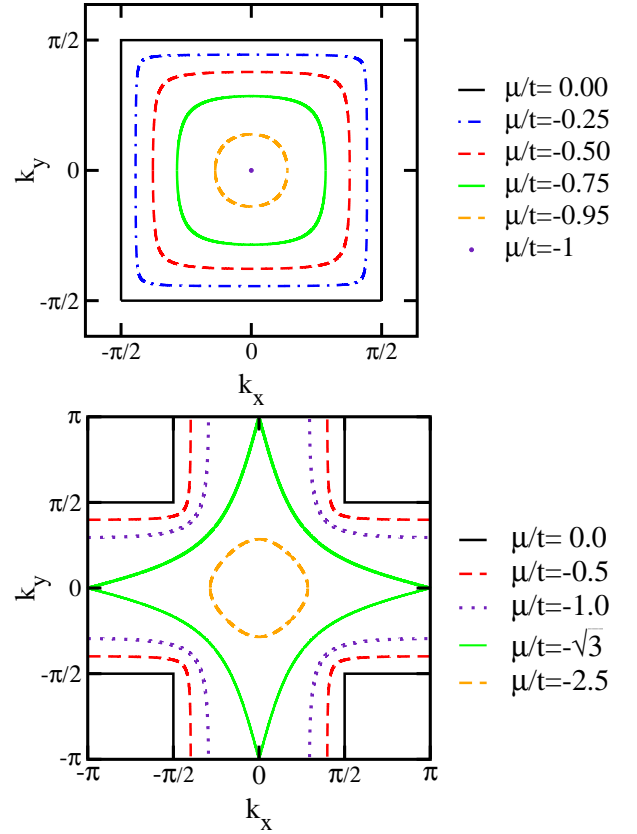


FIG. 1: (Color online) Fermi surfaces of the higher (top) and lower (bottom) bands, as obtained for different values of the chemical potential μ in the two-band tight-binding model for degenerate e_g orbitals ($E_z = 0$). Note a different scale for both Fermi surfaces.

Some of the richness of the present model (1) can be traced back to the peculiar features of the electronic dispersion for e_g electrons in two dimensions.⁶⁸ Unlike for spins, two bands obtained by diagonalizing the Hamiltonian (1) in the noninteracting limit are nondegenerate (except for some high symmetry directions):⁶⁹

$$\varepsilon_{\mathbf{k},\nu} = -t(X + Y) + \nu t \sqrt{X^2 + Y^2 - XY - \varepsilon(X + Y) + \varepsilon^2}, \quad (7)$$

with $\nu = \pm 1$, $X = \cos k_x$, $Y = \cos k_y$, and

$$\varepsilon = \frac{E_z}{2t}. \quad (8)$$

For $\varepsilon = 0$ the corresponding Fermi surfaces are depicted in Fig. 1. At half filling one piece of the Fermi surface is building a "Swiss cross", while the second one is building a square. The filling of the upper band is then by $1/4$ electron, while that of the lower band is by $3/4$ electron per spin. The Fermi surface of the upper band shrinks rather fast with increasing doping x and below $\mu = -t$ ($x = 0.93$) one finds that this band is empty and all electrons are in the lower band. However, both bands are partly filled in the doping regime $x < 0.4$ relevant for

the nickelates, and they will both play a role also when electron interactions are included.

At half filling the edges of the pieces of the Fermi surface (FS) for both bands are connected by the nesting vectors: $\mathbf{Q}_1 = (0, \pi)$ and $\mathbf{Q}_2 = (\pi, 0)$. At the same time, the edges of one piece are connected to the edges of the other one by the nesting vector $\mathbf{Q}_3 = (\pi, \pi)$. In addition, at half filling both components of the velocities vanish on their respective Fermi surfaces. Therefore, several competing instabilities are expected once the interaction is turned on. Their relative importance can be estimated by computing the spin-spin correlation function in the noninteracting limit for the corresponding wave-vectors. In the static limit it reads:

$$\chi_S(\mathbf{Q}) = \frac{2}{N} \sum_{\mathbf{k}} \sum_{\alpha\beta\mu\nu} \frac{f_F(\varepsilon_{\mathbf{k}\mu}) - f_F(\varepsilon_{\mathbf{k}+\mathbf{Q}\nu})}{\varepsilon_{\mathbf{k}+\mathbf{Q}\nu} - \varepsilon_{\mathbf{k}\mu}} \times U_{\alpha\mu}(\mathbf{k}) U_{\mu\beta}^\dagger(\mathbf{k}) U_{\beta\nu}(\mathbf{k} + \mathbf{Q}) U_{\nu\alpha}^\dagger(\mathbf{k} + \mathbf{Q}). \quad (9)$$

Here the matrices $U(\mathbf{k})$ diagonalize the hopping matrix Eq. (3), and $\varepsilon_{\mathbf{k}\mu}$ are given by Eq. (7).

Since ferromagnetism is an expected feature of the model (1), we also evaluate the homogeneous spin-spin correlation functions. It shows an intricate interplay of all the three instabilities (see Fig. 2). They were all reported, regardless of the approach, see for instance Refs. 63 and 67. One finds that the van Hove singularity takes place at $\mu = -\sqrt{3 + \varepsilon^2}t$ for the crystal-field splitting ε , see Eq. (8). At this point the line where the velocity vanishes has a large component on the FS, and the singularity is logarithmic. Note that there is no nesting vector connecting different pieces of the FS, as can be understood by looking at Fig. 1. Here one finds a distinct difference between the present e_g model and the DDH model, where instead the FS is nested and takes the shape of a square for both bands at the van Hove point (for $x = 0$). Therefore, nesting and van Hove singularities in the e_g electron model influence the physical properties at different electron densities than in the DDH model.

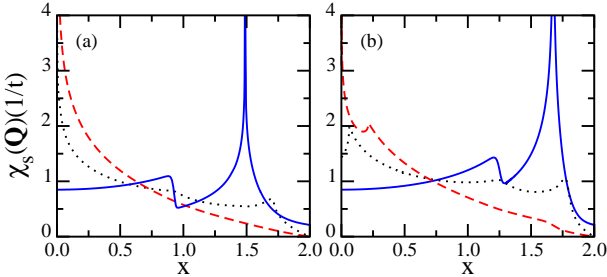


FIG. 2: Static spin-spin correlation functions $\chi_S(\mathbf{Q})$ for e_g electrons for increasing doping, as obtained for: (a) $E_z = 0$, and (b) $E_z = t$. Different lines correspond to: $\mathbf{Q} = (0, 0)$ (solid line), $\mathbf{Q} = (0, \pi)$ (dotted line), and $\mathbf{Q} = (\pi, \pi)$ (dashed line). Van Hove singularity for $\mathbf{Q} = (0, 0)$ is obtained at doping higher than that realized experimentally in nickelate LSNO oxides: (a) $x \simeq 1.49$, and (b) $x \simeq 1.68$.

In the following the Hamiltonian given by Eq. (1) is treated in the HF approximation. We introduce explicitly four "diagonal" expectation values, $\langle n_{i\alpha\sigma} \rangle$, and four "off-diagonal" ones, $\langle c_{i\alpha\sigma}^\dagger c_{i\beta\sigma} \rangle$, with $\alpha, \beta = x, z$ and $\alpha \neq \beta$, that we determine self-consistently in order to get a complete characterization of the ground state. Due to symmetry the last four Fock averages vanish for a 2D square lattice, and one gets the simpler MF Hamiltonian:

$$H_{\text{MF}} = \sum_{ij, \alpha\beta, \sigma} c_{i\alpha\sigma}^\dagger M_{ij, \alpha\beta, \sigma} c_{j\beta\sigma}, \quad (10)$$

with,

$$M_{ij, \alpha\beta, \sigma} = t_{ij}^{\alpha\beta} + \delta_{ij} \delta_{\alpha\beta} M_{i\alpha\sigma}, \quad (11)$$

and,

$$\begin{aligned} M_{ix\sigma} &= \frac{1}{4} \sum_i [(3U - 5J_H) \langle n_i \rangle - \lambda_\sigma (U + J_H) \langle m_i \rangle \\ &\quad - (U - 5J_H) \langle o_i \rangle - \lambda_\sigma (U - J_H) \langle p_i \rangle] + \frac{1}{2} E_z, \\ M_{iz\sigma} &= \frac{1}{4} \sum_i [(3U - 5J_H) \langle n_i \rangle - \lambda_\sigma (U + J_H) \langle m_i \rangle \\ &\quad + (U - 5J_H) \langle o_i \rangle + \lambda_\sigma (U - J_H) \langle p_i \rangle] - \frac{1}{2} E_z, \end{aligned} \quad (12)$$

where we introduced $\lambda_\sigma = \pm 1$ for $\sigma = \uparrow (\downarrow)$ spin and $\lambda_\alpha = \pm 1$ for $\alpha = x(z)$ orbital, and the operators:

$$\begin{aligned} n_i &= \sum_{\alpha\sigma} n_{i\alpha\sigma}, \\ m_i &= \sum_{\alpha\sigma} \lambda_\sigma n_{i\alpha\sigma}, \\ o_i &= \sum_{\alpha\sigma} \lambda_\alpha n_{i\alpha\sigma}, \\ p_i &= \sum_{\alpha\sigma} \lambda_\alpha \lambda_\sigma n_{i\alpha\sigma}, \end{aligned} \quad (13)$$

for total charge and magnetization density, and for orbital anisotropy in the charge and magnetization distribution, respectively.

III. GROUND STATE ENERGIES

Site centered and bond centered stripes represent equally relevant candidates for the ground state. However, it numerically turns out that the energy of SC stripes is substantially larger than the one of the BC stripes, in agreement with the early study of Yi et al.⁶² (see Table III in Sec. V as well). We therefore concentrate on BC stripes. They are made out of pairs of atoms with a FM spin polarization within the model Hamiltonian (1) in the wide doping regime $0.05 \leq x \leq 0.4$. In order to obtain unbiased results, we performed calculations on large clusters implementing the symmetry of stripe phases in reciprocal space. We worked on squared

clusters with the linear dimension along the x direction chosen as an *even* multiplicity of the elementary stripe unit cell dimension. Their sizes are listed in Table I.

To ensure that the model (1) is indeed relevant for the nickelates, it is necessary to focus on appropriate values of parameters U , J_H , and E_z . First of all, x-ray absorption (XAS) measurements⁷⁰ as well as from XPS and bremsstrahlung-isochromat spectroscopy studies⁷¹ of the electronic structure of LSNO suggest that LSNO is a CT insulator with nearly the same CT energy Δ as that of NiO. Therefore, the same parameters could be accepted as used before in the self-consistent Born calculations,⁷² which reproduced quite well photoemission spectra of NiO. Secondly, since our approximation has a tendency to overestimate the effect of the Coulomb repulsion in LSNO, we used a somewhat smaller value of the Coulomb repulsion U than that adequate for NiO, i.e., we set $U = \Delta = 5$ eV. Next, as the in-plane Ni–O–Ni bond length in La_2NiO_4 of 1.95 Å (see Ref. 65) is very much the same as the shorter bond of 1.89 Å in La_2CuO_4 ,⁶⁶ we set the hopping amplitude t_{pd} between the p_σ orbitals and $|x\rangle \sim |x^2 - y^2\rangle$ orbitals to be as in LSCO, i.e., $t_{pd} = 1.47$ eV.⁷³ This in turn yields an effective in-plane Ni–Ni hopping $t^{xx} = (t_{pd}^2/\Delta) = 0.43$ eV. However, it is more convenient to take the effective ($dd\sigma$) hopping element connecting two $|z\rangle \sim |3z^2 - r^2\rangle$ orbitals along the c -axis as the energy unit t , related to t^{xx} via the Slater-Koster relation $t = 4t^{xx}/3 \simeq 0.6$ eV, so that $U \simeq 8t$.

The value of Hund's exchange between t_{2g} electrons in NiO was estimated as $J'_H = 0.8$ eV.⁷⁴ It is related to J_H

TABLE I: Comparison of the ground state free energy F for the VBC (left) and DBC (right) stripe phases as found in the e_g model for increasing doping x . Stripes are separated by $d = 3, \dots, 11$ lattice constants in clusters of size $L \times L$. Parameters: $U = 8t$, $J_H = 1.5t$ and $E_z = 0$.

VBC				DBC		
x	d	$L \times L$	F/t	d	$L \times L$	F/t
0.05	11	88×88	2.8811	11	88×88	2.8794
0.06	11	88×88	2.8376	11	88×88	2.8326
0.07	11	88×88	2.7946	11	88×88	2.7870
0.08	11	88×88	2.7519	11	88×88	2.7430
0.09	10	80×80	2.7099	10	80×80	2.7001
0.10	10	80×80	2.6677	9	72×72	2.6570
0.11	9	72×72	2.6258	8	64×64	2.6140
0.12	8	64×64	2.5839	7	84×84	2.5712
0.14	7	84×84	2.5001	6	72×72	2.4853
0.16	6	72×72	2.4162	6	72×72	2.3997
0.18	5	80×80	2.3329	5	80×80	2.3130
0.20	5	80×80	2.2485	4	80×80	2.2291
0.25	4	80×80	2.0394	4	80×80	2.0155
0.30	3	72×72	1.8325	3	72×72	1.8029
0.40	3	72×72	1.4619	3	72×72	1.4081

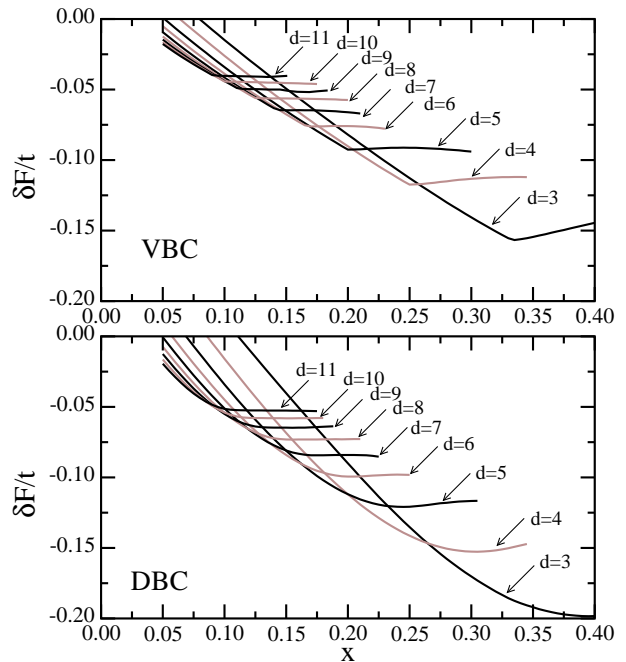


FIG. 3: Free energy gains δF (15) of the VBC (top) and DBC (bottom) stripe phases with respect to the AF phase (15) as functions of doping x , obtained at temperature $\beta t = 100$ for the e_g model. Cluster sizes, distances between DWs d , and parameters are the same as in Table I.

for e_g electrons through the simple relation,⁷⁵

$$J_H = J'_H + B, \quad (14)$$

where B stands for a Racah parameter.⁷⁶ Taking into account that $B \simeq 0.13$ eV for NiO_2 ,⁷⁷ one finds $J_H = 0.93$ eV, i.e., $J_H \simeq 1.5t$. Indeed, it has been shown that $J_H = 1$ eV reproduces the experimental band gap and the magnetic moment of La_2NiO_4 .⁷⁸ Finally, we set $E_z = t = 0.6$ eV as a realistic value of the crystal field splitting in the nickelates. On the one hand, band structure calculations in the local density approximation predict the crystal field splitting between e_g orbitals to be 0.5 eV.⁷⁹ On the other hand, XAS spectra reveal a somewhat larger splitting of 0.7 eV,⁸⁰ a value also deduced from the optical spectroscopy.³⁹

The performed calculations demonstrate a robust tendency towards stripe formation expressed by negative free energy gains of the vertical bond-centered (VBC) and diagonal bond-centered (DBC) stripe phases with respect to the AF phase,

$$\delta F \equiv F_S - F_{AF}, \quad (15)$$

for the e_g model (1). This energy gain $|\delta F|$ increases with doping x , as shown in Fig. 3. The δF curves cross each other for decreasing distances between DWs d which demonstrates the tendency to the gradual formation of stripe phases with smaller unit cells upon increasing doping. Thereby, diagonal structures are significantly lower

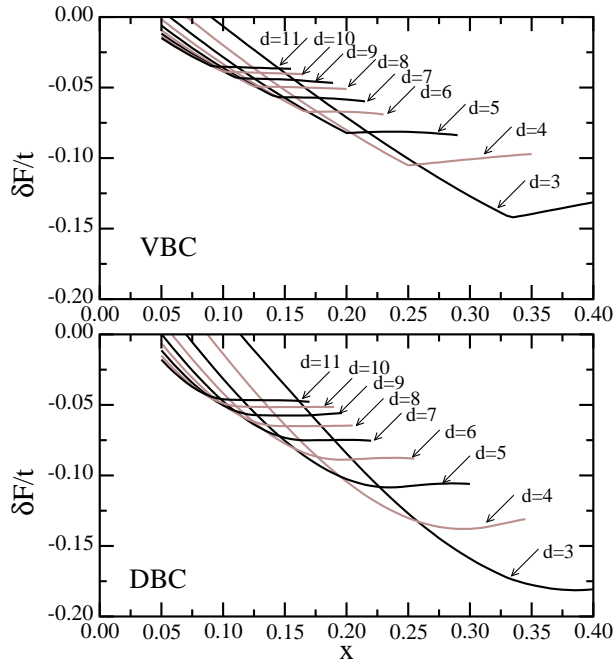


FIG. 4: Free energy gains δF as in Fig. 3, but with finite crystal field splitting $E_z = t$. Cluster sizes, distances between DWs d , and parameters are the same as in Table I.

in energy than vertical ones for a given fixed doping, but especially in the large doping regime $x \sim 0.4$. The robust stability of the DBC stripe phases with respect to the VBC ones is illustrated more transparently in Table I, where we compare the ground state free energy F for both structures. Note that a similar variation of the optimal distance d between DWs suggests the same optimal stripe filling.

The main effect of the crystal field splitting is to reduce the stability of both stripe phases with respect to the uniform AF phase. This appears to be rather puzzling at first sight. One finds, however, that realistic positive E_z promotes the $|z\rangle$ orbitals with a narrow band. On the one hand, the electron distribution induced by finite E_z suppresses substantially the AF superexchange energy gain which becomes $J_{zz} = 4t_{zz}^2/U$ rather than $J_{xx} = 4t_{xx}^2/U$. On the other hand, one would expect that such charge redistribution strongly increases the kinetic energy gain due to a wider band accessible for holes, propagating especially easily along DWs where the AF order is partly suppressed. Nevertheless, this energy gain is easily overcompensated by the kinetic energy loss due to hopping perpendicular to the stripes. In addition, our studies of the BC stripe phases within the single-band Hubbard model have shown that the largest kinetic energy gain is released on the bonds connecting pairs of ferromagnetically coupled atoms located in the DWs.²⁴ Note that the FM order of the DW spins is substantially stabilized by the off-diagonal t_{xz} hopping in the e_g model, yielding low-energy charge excitations that lead to the FM superexchange, $J_{xz} = 4t_{xz}^2/(U - 3J_H)$. Altogether, when

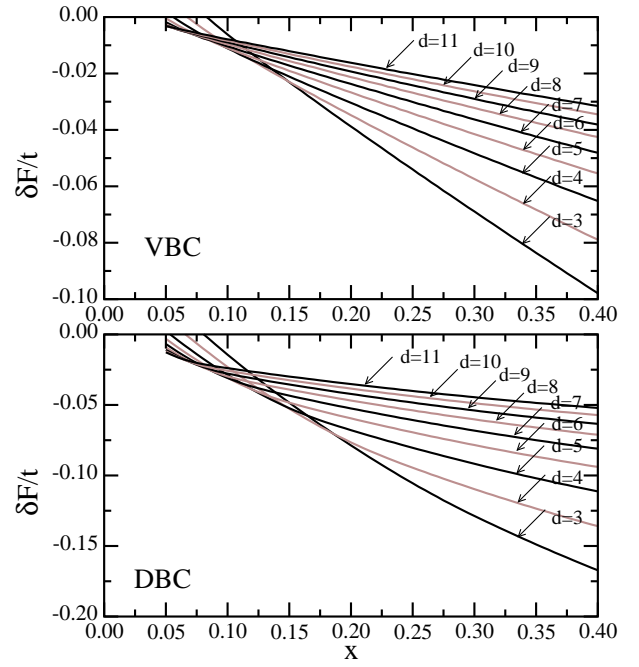


FIG. 5: Free energy gains δF of the VBC (top) and DBC (bottom) stripe phases with unit cells of length d , as a function of doping x , obtained for the DDH model. Parameters: $U = 8t$, $J_H = 1.5t$, $E_z = 0$, and $\beta t = 100$.

one orbital is sufficiently favored by finite crystal field over the other one, these low-energy processes are effectively blocked, explaining the enhanced stability of the AF order with respect to the BC solutions (*cf.* Figs. 3 and 4).

A further qualitative point concerns the influence of a finite crystal field splitting E_z between the $|x\rangle$ and $|z\rangle$ orbitals on the stability of DW structures. As depicted in Fig. 4, a more realistic value $E_z = t$ seems not to promote noticeably any stripe phase over another one and one still recovers DBC stripe phases as the ground state. We therefore conclude that it is not the crystal field E_z that is responsible for a different orientation of DWs in the nickelates from that observed in the cuprates. Later on we shall see that finite E_z has also only a little visible effect on optimal stripe filling.

Let us now shortly return to the experimental characterization of the stripe phases in LSNO. Their periodicity at a given doping x is described by both charge $\mathbf{Q}_c = \pm\pi(2\epsilon, 2\epsilon)$ and spin $\mathbf{Q}_s = \pi(1 \pm \epsilon, 1 \pm \epsilon)$ wave vectors along the direction diagonal with respect to the Ni–O bond. The incommensurability ϵ corresponds to the inverse of the distance d between DWs,^{1,2,3,4,5,6,7,8} i.e.,

$$\epsilon = \frac{1}{d}. \quad (16)$$

Further, ϵ first increases continuously with doping x and follows the linear relation $\epsilon = x$ in the wide doping range $x \leq 1/3$, while next it gradually saturates to the value $\epsilon \simeq$

0.44.⁸ Such a behavior of ϵ indicates a fixed hole density of one hole per Ni ion in a DW, and is consistent with the HF predictions both in the single and in multiband models.^{19,20,21,22,23,60,61,62} Finally, a fixed hole density along the DWs results in the pinning of the chemical potential μ for $x \leq 1/3$, whereas a large ($\simeq 1$ eV/hole) downward shift appears in the higher doping regime.⁴⁶

It is interesting to establish whether the above results concerning the stripe phases in the ground state and their variation under increasing doping appear solely in the realistic e_g model, or they are generic and remain also a common feature of the DDH model with only diagonal hopping elements given by Eq. (6). To allow a meaningful comparison, we set the same values of microscopic parameters as we those chosen for the e_g model, i.e., $U = 8t$, $J_H = 1.5t$, and we consider only the $E_z = 0$ case imposed by symmetry between the equivalent orbitals. It restricts the solutions of the DDH model to $\langle o \rangle = \langle p \rangle = 0$ (see below).

One finds that the free energy gains δF of the VBC and DBC stripe phases with respect to the AF phase for the DDH model (Fig. 5) are qualitatively similar to those of the e_g band model. First of all, for a fixed doping x diagonal stripe structures are again significantly lower in energy than vertical ones (*cf.* also Table II). Secondly, also in this case, we recover a gradual crossover towards stripe phases with smaller unit cells upon increasing doping. Note, however, that in contrast to the predictions made within the e_g model, structures with vertical (diag-

onal) DWs separated by a distance $d \geq 5$ are the lowest energy solutions only in a narrow doping regime $x \lesssim 0.12$ ($x \lesssim 0.15$), respectively.

For a complete characterization of stripe phases we define

$$\nu = \frac{N_h}{LN_{\text{DW}}}, \quad (17)$$

where N_h is the number of doped holes and N_{DW} is the number of domain walls. Our findings concerning the properties of BC stripe phases are summarized in Fig. 6 showing the doping dependence of the incommensurability ϵ , the stripe filling ν , and the chemical potential μ for both the VBC (left) and DBC (right) stripe phases. These quantities for the respective ground states are deduced from Figs. 3, 4 and 5. In each case the data points correspond to the middle of the stability region of the stripe phase of a given type. The only exception are the $d = 3$ phases — for them ϵ , ν , and μ , are plotted for the actual minimum of the free energy F .

In agreement with the experimental data for LSNO, indicated here by a solid line in panels (a) and (b) of Fig. 6, one observes that ϵ follows the law $\epsilon \simeq x$ up to $x \simeq 0.2$ and then it tends to saturate to the highest possible value for the BC stripe phase, i.e., $\epsilon = 1/3$, as there are no BC stripe phases in which DWs are separated by $d = 2$ lattice spacings. Further, in the regime where ϵ follows linearly the doping level x , decreasing stripe periodicity allows the system to maintain nearly fixed filling ν [*cf.* Figs. 6(c) and 6(d)], pinning simultaneously the chemical potential μ , as shown in Figs. 6(e) and 6(f). Remarkably, the ground state of both the VBC and DBC stripe phases is characterized by the optimal filling 0.9 hole/Ni, very close indeed to the experimental value one hole/Ni ion, and the optimal filling remains almost unaltered in the model with a finite crystal field $E_z = t$.

Regarding the chemical potential shift $\Delta\mu$ in the doping regime $x > 0.2$, one finds that it exceeds the experimental value ~ -1.0 eV/hole nearly by a factor of 2. Indeed, assuming the effective hopping $t = 0.6$ eV, one obtains $\Delta\mu \simeq -2.2$ (-2.1) eV/hole for $E_z = 0$ ($E_z = t$), respectively. Therefore, we conclude that the present effective model can only explain qualitative trends and one needs to carry out calculations within more realistic multiband models with oxygen orbitals included explicitly in order to obtain quantitatively the experimental data.

Let us verify now whether the established results concerning the doping dependence of ϵ and ν are also obtained within the DDH model. As the structures with vertical (diagonal) DWs separated by a distance $d \geq 5$ appear in the DDH model only in a narrow doping regime $x \lesssim 0.12$ ($x \lesssim 0.15$), respectively, one observes here a fast variation of the optimal distance d which should result in a small optimal stripe filling. Indeed, as depicted in Figs. 6(a) and 6(b), the low-doping part of ϵ , being linear in x , has a larger slope which exceeds the experimental value in LSNO roughly by a factor of 2 (1.5) in the case of the

TABLE II: Comparison of the ground state free energy F per site for the VBC (left) and DBC (right) stripe phases as found in the DDH model for increasing doping x . Stripes are separated by d lattice constants in clusters of size $L \times L$. Parameters: $U = 8t$, $J_H = 1.5t$, and $E_z = 0$.

x	VBC			DBC		
	d	$L \times L$	F/t	d	$L \times L$	F/t
0.050	11	88×88	3.1095	11	88×88	3.1000
0.055	10	80×80	3.0912	11	88×88	3.0804
0.060	9	72×72	3.0729	11	88×88	3.0610
0.065	8	64×64	3.0547	10	80×80	3.0417
0.070	8	64×64	3.0364	9	72×72	3.0225
0.080	8	64×64	3.0001	8	64×64	2.9839
0.090	7	84×84	2.9636	7	84×84	2.9454
0.100	6	72×72	2.9269	7	84×84	2.9070
0.110	5	80×80	2.8902	6	72×72	2.8683
0.120	4	80×80	2.8538	5	80×80	2.8301
0.140	4	80×80	2.7807	5	80×80	2.7530
0.160	3	72×72	2.7077	4	80×80	2.6760
0.180	3	72×72	2.6347	4	80×80	2.5996
0.200	3	72×72	2.5626	3	72×72	2.5227
0.300	3	72×72	2.2129	3	72×72	2.1531
0.400	3	72×72	1.8809	3	72×72	1.8116

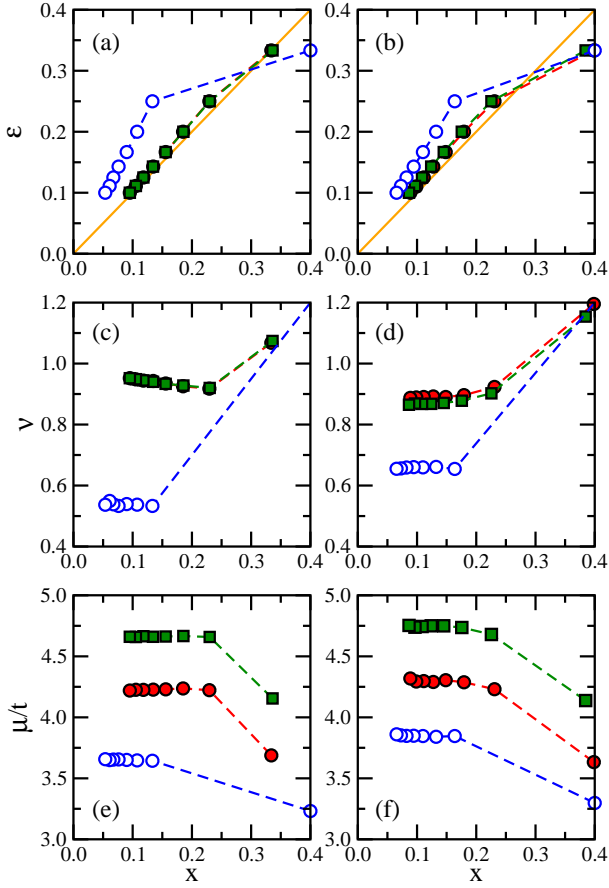


FIG. 6: (Color online) Doping dependence of stripe phases for the VBC (left) and DBC (right) ground states: (a) and (b) magnetic incommensurability ϵ ; (c) and (d) stripe filling ν ; (e) and (f) chemical potential μ (in the units of t), as deduced from the data of Figs. 3, 4 and 5. Filled (open) symbols for e_g (DDH) model; circles and squares for $E_z = 0$ and $E_z = t$. Solid lines in panels (a) and (b) show the experimental behavior of ϵ in LSNO given in Ref. 8.

VBC (DBC) stripe phase, respectively. Consequently, the optimal stripe filling in the former case is substantially reduced down to $\nu \simeq 0.55$ and in the latter case — down to $\nu \simeq 0.65$ [see Figs. 6(c) and 6(d)]. Finally, one finds that the chemical potential starts to decrease rapidly at $x \simeq 0.14$ in the VBC stripe phase [Fig. 6(e)] and at slightly larger doping $x \simeq 0.16$ in the DBC phase [Fig. 6(f)].

IV. MECHANISM OF STRIPE FORMATION

A. Charge and magnetization distributions in the stripe phases

In order to find out the reason of such a vast discrepancy between the predictions made in the e_g and in the DDH model, let us now investigate closer the properties of idealized filled and half-filled DWs: half-filled

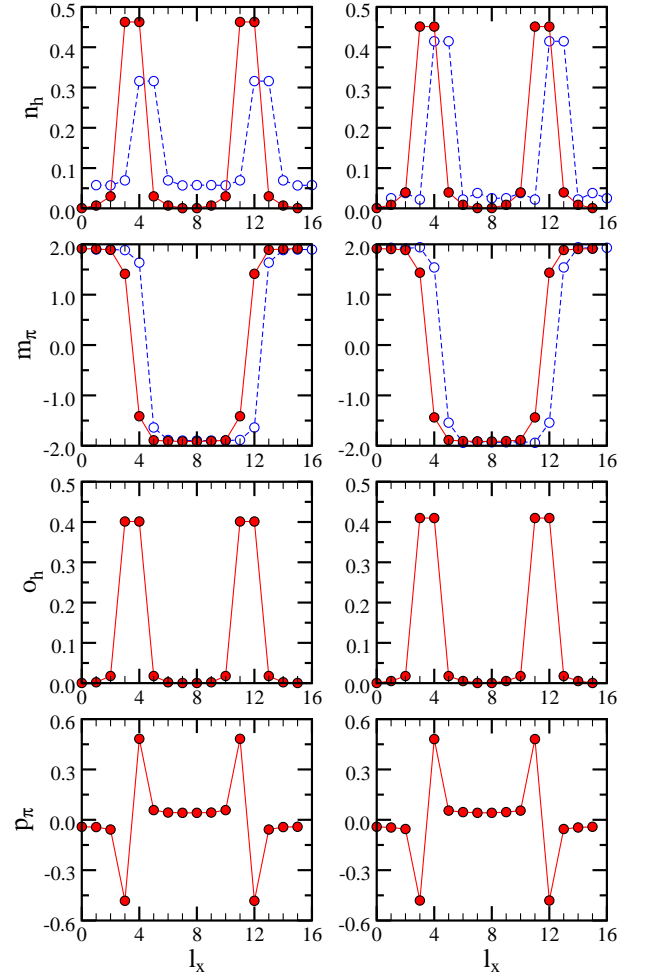


FIG. 7: (Color online) Charge and magnetization distribution in the filled VBC (left) and DBC (right) stripe phase found in either the e_g model (filled circles), or in the DDH model (open circles) on a 64×64 cluster at doping $x = 1/8$: local hole densities $n_h(l_x)$ (top row); modulated magnetization densities $m_\pi(l_x)$ (second row); local hole $o_h(l_x)$ (third row); and local modulated magnetic $p_\pi(l_x)$ orbital polarization (bottom row). For more clarity, the data points for the DDH model are shifted by one lattice constant from the origin of the coordinate system. Parameters: $U = 8t$, $J_H = 1.5t$, $E_z = 0$, and $\beta t = 100$.

vertical bond-centered (HVBC) and half-filled diagonal bond-centered (HDBC). A complete characterization of the charge and magnetization distributions for a system with orbital degeneracy is given by: the local hole density $x(l_x)$, local modulated magnetization density $m_\pi(l_x)$, local hole orbital polarization $o_h(l_x)$, and local modulated magnetic orbital polarization $p_\pi(l_x)$, defined using the

operators given in Eqs. (13) as follows:

$$\begin{aligned}
 n_h(l_x) &= \sum_{\alpha} n_{h\alpha}(l_x), \\
 m_{\pi}(l_x) &= (-1)^{l_x} \sum_{\alpha\sigma} \lambda_{\sigma} n_{\alpha\sigma}(l_x), \\
 o_h(l_x) &= \sum_{\alpha} \lambda_{\alpha} n_{h\alpha}(l_x), \\
 p_{\pi}(l_x) &= (-1)^{l_x} \sum_{\alpha\sigma} \lambda_{\alpha} \lambda_{\sigma} n_{\alpha\sigma}(l_x).
 \end{aligned} \tag{18}$$

Here $n_{\alpha\sigma}(l_x)$ is the local orbital charge density for spin σ , whereas $n_{h\alpha}(l_x)$ denotes the local orbital hole density,

$$n_{h\alpha}(l_x) = 1 - \sum_{\sigma} n_{\alpha\sigma}(l_x). \tag{19}$$

To better appreciate the differences between the DDH and the e_g model, we compare in Fig. 7, the local hole $n_h(l_x)$ and the modulated magnetization densities $m_{\pi}(l_x)$ of the filled VBC and DBC stripe phases found at temperature $\beta t = 100$ in either model on a 64×64 cluster at doping $x = 1/8$ for the standard parameters, *i.e.*, $U = 8t$, $J_H = 1.5t$, and $E_z = 0$. For completeness we also show the local hole $o_h(l_x)$ and the local modulated magnetic $p_{\pi}(l_x)$ orbital polarization. These quantities are finite only in the e_g model, while $o_h(l_x) = p_{\pi}(l_x) = 0$ by symmetry in the DDH model. Since o_h is positive the holes are located in $|x\rangle$ orbitals, and the polarization of the two sites on the DWs is FM (alternation of signs in p_{π} at the DWs).

The observed differences, especially pronounced at DW atoms, directly follow from the fact that, a different effect helping to reduce double occupancy at those sites is effective in each model. Namely, in the e_g hopping model (3) one finds large positive $o_h(l_x)$ at DWs, which means that it is energetically advantageous to optimize the kinetic energy of holes by putting them into the $|x\rangle$ orbitals where the hopping element t_{xx} is larger and gives a wide band. On the one hand, in the HF the only way to optimize the on-site energy is to develop a strong spin polarization which, in turn, would noticeably reduce the kinetic energy gain. On the other hand, such disadvantageous suppression can be avoided by a strong reduction of the electron density. This explains why the hole density $n_h(l_x)$ along DWs in the e_g model is larger, as compared to the corresponding value found in the DDH case. Indeed, in the latter case both bands are equivalent, resulting in $o_h(l_x) = p_{\pi}(l_x) = 0$. Hence this model yields a more localized stripe phase with a larger magnetization $|m_{\pi}(l_x)|$ at DWs than the one obtained in the e_g model (*cf.* Fig. 7).

For completeness, in Fig. 8 we compare the hole density, $n_h(l_x)$, and the spin density, $m_{\pi}(l_x)$, profiles of the half-filled stripe phases. The unit cells are smaller by a factor of two and the amplitude of the charge density wave is correspondingly reduced. Even though the overall shape of the DWs looks very much the same in both

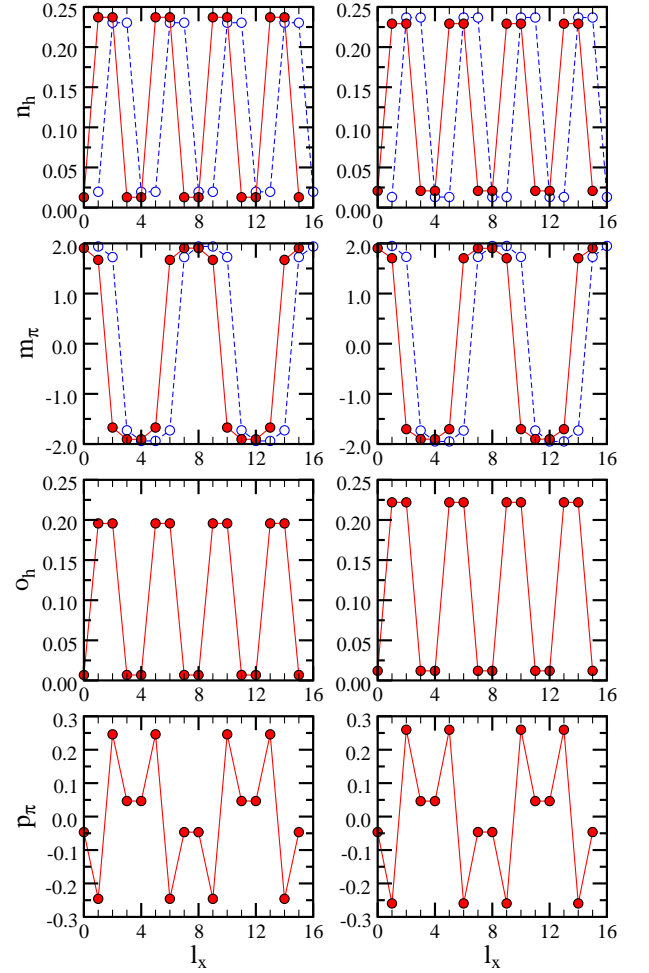


FIG. 8: (Color online) Charge and magnetization distributions in the half-filled HVBC (left) and HDBC (right) stripe phases found in either the e_g (filled circles) model, or in the DDH model (open circles) on a 64×64 cluster at doping $x = 1/8$. The meaning of the different panels and shift of the DDH data as in Fig. 7. Parameters: $U = 8t$, $J_H = 1.5t$, $E_z = 0$, and $\beta t = 100$.

models, a larger magnetization $|m_{\pi}(l_x)|$ at DWs is found again within the DDH Hamiltonian (6).

B. Double occupancy distribution

Furthermore, important information about the nature of stripe phases is provided by the averaged intraorbital double occupancy at site l_x ,

$$D(l_x) = \sum_{\alpha} n_{\alpha\uparrow}(l_x) n_{\alpha\downarrow}(l_x), \tag{20}$$

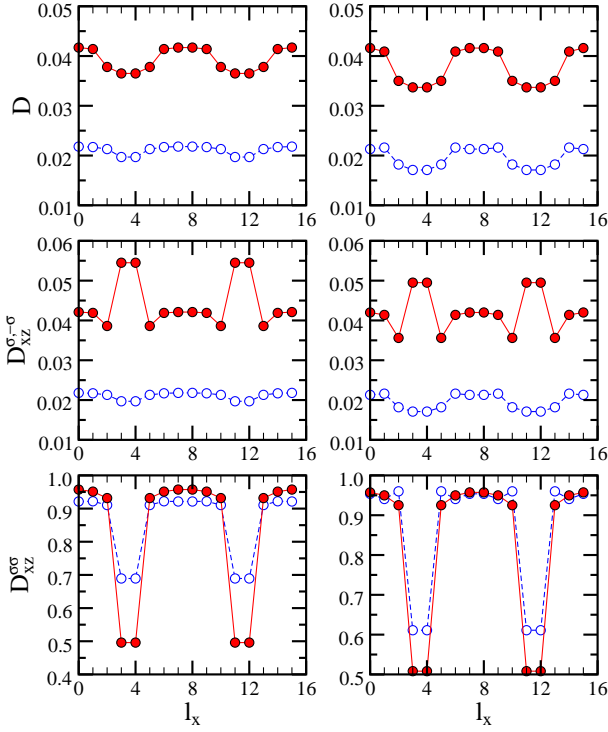


FIG. 9: (Color online) Double occupancy distribution in the filled VBC (left) and DBC (right) stripe phase shown in Fig. 7: intraorbital double occupancy $D(l_x)$ (top row), and two local interorbital $D_{xz}^{\sigma\bar{\sigma}}(l_x)$ (middle) and $D_{xz}^{\sigma\sigma}(l_x)$ (bottom) double occupancies. Filled (open) circles denote the results found in the e_g (DDH) model, respectively. Parameters and filled/empty circles as in Fig. 7.

as well as by two local interorbital double occupancies,

$$D_{xz}^{\sigma\bar{\sigma}}(l_x) = \sum_{\sigma} n_{x\sigma}(l_x) n_{z\bar{\sigma}}(l_x), \quad (21)$$

$$D_{xz}^{\sigma\sigma}(l_x) = \sum_{\sigma} n_{x\sigma}(l_x) n_{z\sigma}(l_x), \quad (22)$$

where $\bar{\sigma} = -\sigma$. In a system with isotropic charge distribution the double occupancies are site independent, while in stripe phases they vary with a characteristic periodicity following from the size of the stripe unit cell. From the structure of the Coulomb interaction Eq. (4) one expects $D < D_{xz}^{\sigma\bar{\sigma}} < D_{xz}^{\sigma\sigma}$ for a fixed hole density. In a stripe phase these double occupancies are locally suppressed by the magnetic and orbital polarizations in a way that depends both on the shape of the stripe, and on the form of the one-electron Hamiltonian. Let us first discuss the average double occupancies (20)-(22) of the stripe phases depicted in Fig. 7. Remarkably, in the DDH model (open circles in Fig. 9) the on-site energy is predominantly optimized by the reduction of the high-energy configurations with opposite spins which lead to intraorbital $D(l_x)$ and interorbital $D_{xz}^{\sigma\bar{\sigma}}(l_x)$ double occupancies, so that the system might create a large number of DWs in the unit cell even in the low doping regime, consequently reducing the optimal stripe filling. Such a strong reduction of the

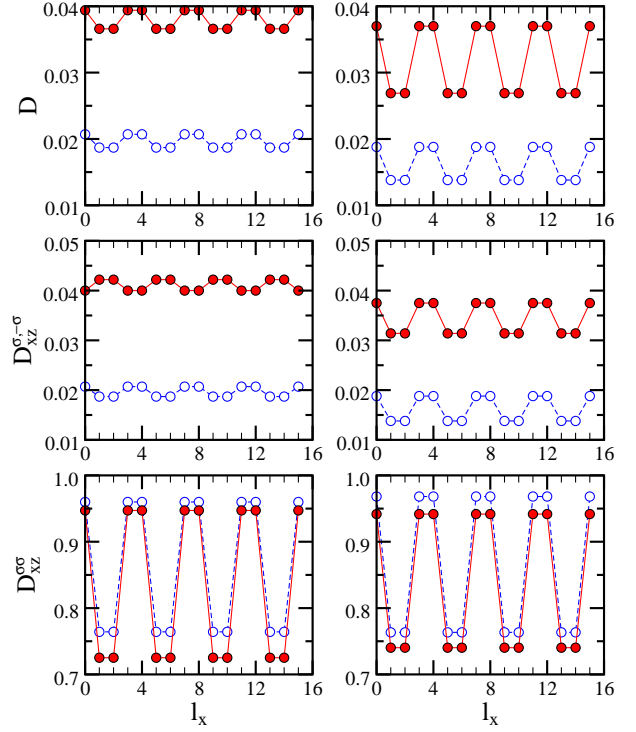


FIG. 10: (Color online) Double occupancy distribution in the half-filled stripe phases shown in Fig. 8: HVBC (left) and HDBC (right). Different double occupancies as in Fig. 9. Parameters and filled/empty circles as in Fig. 8.

double occupancies for opposite spins follows from the diagonal hopping which gives a weaker electronic mixing between the sites of opposite spin due to a lower kinetic energy.⁸²

In contrast, in the e_g model (filled circles in Fig. 9), the Coulomb energy is mainly optimized by the reduction of the low-energy interorbital $D_{xz}^{\sigma\sigma}(l_x)$ double occupancy resulting in a smaller magnetization $|m_{\pi}(l_x)|$ at DWs as compared to the one found in the DDH model. However, reduced $|m_{\pi}(l_x)|$ at those sites allows the system to better optimize the kinetic energy gain which then overcompensates a large on-site energy only when the optimal filling is close to one hole per Ni site, meaning that for a given doping level, the DWs should be separated by a larger distance as compared to predictions made in the DDH model. On the other hand, the robust stability of the DBC stripe phases with respect to the VBC ones can be understood as following from a stronger reduction of all double occupancies (20)-(22) in the former phase. In fact, the doubly occupied configurations cannot be then excited between the nearest neighbor DW sites, leading to a lower total energy.

In case of half-filled stripes (Fig. 10) the double occupancies for opposite spins ($D(l_x)$ and $D_{xz}^{\sigma\bar{\sigma}}(l_x)$) are only slightly lower than for filled stripes, but the interorbital double occupancy for equal spins ($D_{xz}^{\sigma\sigma}(l_x)$) is significantly higher, reflecting the higher electron filling at DW atoms in these phases. Due to the finite Hund's exchange

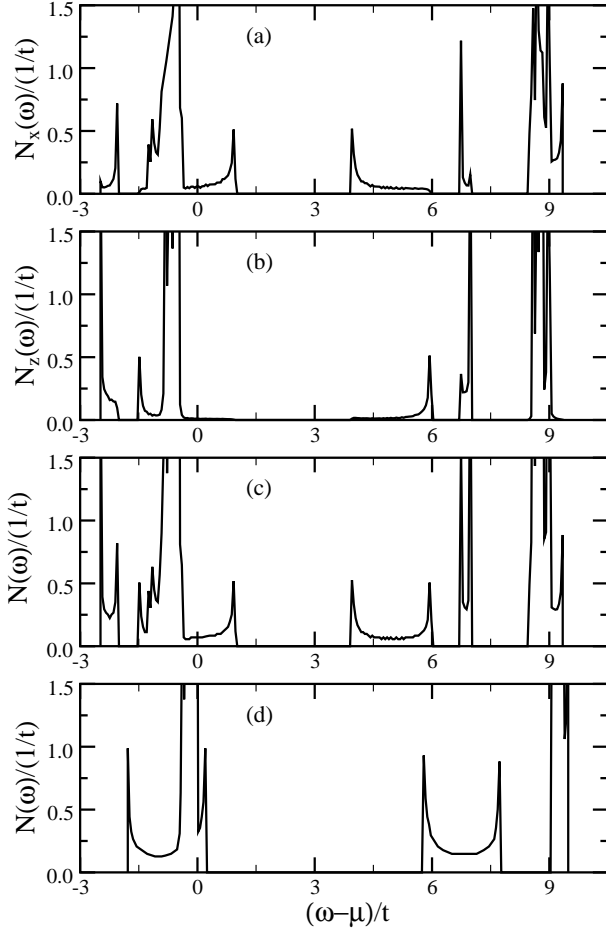


FIG. 11: Densities of states for the DBC stripe phase in the e_g model at $x = 1/8$ doping: (a) partial density of states $N_x(\omega)$ for $|x\rangle$ orbital, (b) partial density of states $N_z(\omega)$ for $|z\rangle$ orbital, (c) total density of states $N(\omega)$. Panel (d) shows for comparison the total density of states $N(\omega)$ as found in the DBC stripe phase within in the DDH model. Parameters as in Fig. 7.

considered here, $J_H = 0.15t$, the high-spin states are promoted. Altogether one finds similar generic features seen above for the filled stripes (Fig. 9): (i) both double occupancies for the opposite spins are stronger reduced in the DDH model, and (ii) the double occupancy by the same spin $D_{xz}^{\sigma\sigma}$ at the DWs is stronger suppressed in the e_g model, resulting from a smaller magnetization at these sites than in the DDH model. This second effects seems to play a role in stabilizing the HDBC stripe phase in the DDH model rather than the DBC phase, found for the realistic e_g model.

C. Densities of states

Important differences between the two models strongly influence the density of states (DOS). Here we first de-

termine the DOS projected on the α orbital as:

$$N_\alpha(\omega) = \frac{1}{N} \sum_{\mathbf{k}} \sum_{i\sigma} |\Psi_{i\alpha\sigma}(\mathbf{k})|^2 \delta(\omega - \varepsilon_{\mathbf{k}\sigma}), \quad (23)$$

where $\Psi_{i\alpha\sigma}(\mathbf{k})$ are the eigenvectors of the MF Hamiltonian Eq. (10). It is calculated using a histogram of the corresponding eigenvalues. It is apparent from Figs. 11 and 12 that the spectra consist of several subbands. However, two Hubbard subbands are well visible both for filled and half-filled diagonal BC stripes: lower Hubbard band (LHB) and upper Hubbard band (UHB). The Hubbard subbands arise primarily due to the AF polarization and the gap between them is proportional to the magnetization.

Panels (a) and (b) in Figs. 11 and 12 show the DOS $N_\alpha(\omega)$ (23), projected on the orbital $|x\rangle$ and $|z\rangle$, respectively. Here, one finds that the mid-gap bands have mainly $|x\rangle$ character close to the gap between them — the $|x\rangle$ orbitals optimize the kinetic energy of holes doped into them, whereas the vast majority of the more localized $|z\rangle$ states of DW atoms belongs to the energy regimes within the LHB and close to the UHB.

The total DOS for the DBC stripes in the e_g model, depicted in Fig. 11(c), reveals mid-gap states which demonstrate the one-dimensional character of the transport in the stripe phases. Note that due to the AF spin modulation along the BC DWs themselves, one finds as well a distinct gap between two mid-gap bands lying within the Mott-Hubbard gap. This gap for the filled DBC stripes is lower in the e_g model [Fig. 11(c)] than in the DDH model [Fig. 11(d)], as the holes are more delocalized in the former case. This holds as well for the HDBC stripes, see Figs. 12(c) and 12(d). We have shown before that the magnetization on the DW sites is larger for the HDBC stripes than for the DBC ones, and therefore the gaps between the mid-gap states are also larger in Fig. 12 than in Fig. 11.

Remarkably, both for the filled and half-filled diagonal BC stripe phases of Figs. 11 and 12 the lower mid-gap states are to some extent localized above the LHB in the e_g model, whereas they are clearly almost merged with the LHB in the DDH model. This behavior follows from a smaller on-wall magnetization $m_\pi(l_x)$ in the e_g model. Therefore, in the DDH case only a few holes occupy the low-lying mid-gap bands, explaining the reason of substantial suppression of the optimal stripe filling in this case. Instead, filled stripes are favored in the e_g model — they have a larger fraction of holes in the lower mid-gap states. Note, however, that also in this case the stripes are metallic, with some spectral weight (mainly in $|x\rangle$ orbitals) above $\omega = \mu$.

V. DISCUSSION AND SUMMARY

We summarize our key results concerning the stability of stripe phases in the nickelates. We investigated

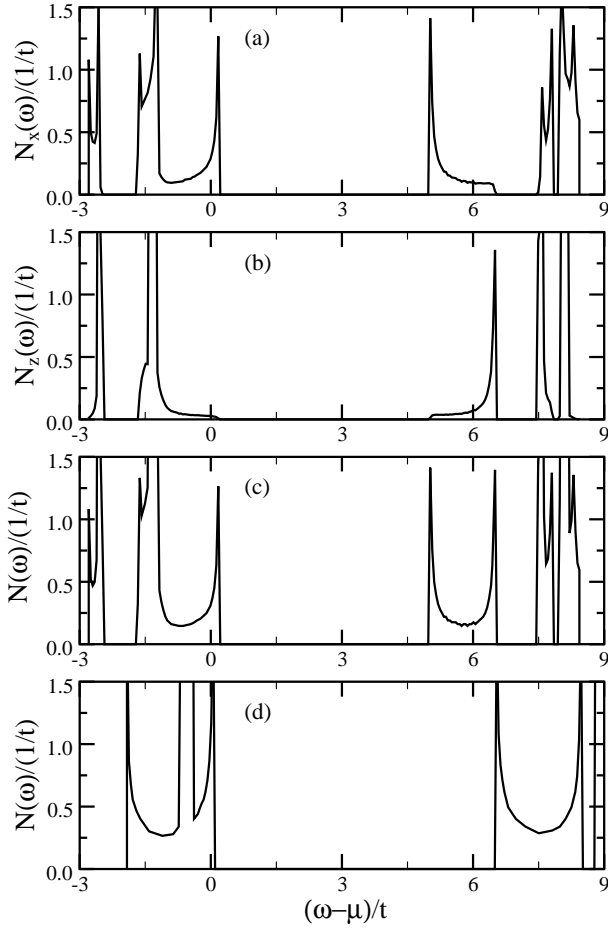


FIG. 12: Densities of states for the HDBC stripe phase in the e_g model at $x = 1/8$ doping, panels (a)-(c) as in Fig. 11. Panel (d) shows for comparison the total density of states $N(\omega)$ as found in the HDBC stripe phase within in the DDH model. Parameters as in Fig. 8.

this problem using two Hubbard models — the realistic model for e_g electrons, and the DDH model which frequently serves as the simplest approach to the orbital degeneracy.⁸¹ It is quite encouraging that the DDH model gives already diagonal stripe phases as the most stable structures, in contrast to the nondegenerate Hubbard model where the vertical (horizontal) stripes are found in the HF approximation. However, one finds half-filled BC stripes in the DDH model, and it is only in the realistic e_g model for doped nickelates that one observes a generic tendency to promoting filled stripes over the half-filled ones. As an example of this behavior, we give the free energies of filled and half-filled stripe phases found within both (e_g and DDH) models for $x = 1/8$ doping in Table III. First of all, one finds that the energies of BC phases are considerably lower for the realistic model of e_g band due to the higher kinetic energy gains which result from the off-diagonal hopping.⁸² Most importantly, for the parameters relevant to LSNO used for the data of Table III, one finds that the DBC phase has

the lowest energy, *i.e.*, indeed experimentally observed *filled* diagonal stripes. In contrast, the SC stripe phases with unpolarized DW sites and large double occupancies have much higher energies, and the best of them is not diagonal, but vertical (horizontal) one. We also note that even though the DDH model with two equivalent orbitals clearly favors diagonal DWs, it stabilizes instead of filled the *half-filled* diagonal phases.

As in the cuprates, the coexisting charge and magnetic order in diagonal stripe phases in the nickelates is a result of the compromise between the kinetic and magnetic energies — the magnetic energy is gained in the AF domains, and the kinetic energy is gained mainly along the DWs. The BC stripes are favored as then the magnetic energy can be gained (Table III) not only in the AF domains, but also on the DW magnetic sites. Finally, when the DWs are filled, more kinetic energy is gained in the e_g model while then the off-diagonal hopping is allowed. Altogether, this mechanism shows little sensitivity to the small crystal field splitting. For moderate values of the latter it tends to eliminate stripe phases entirely rather than promoting one stripe phase over another one.

In spite of the remarkable success of the present study which gave stable diagonal stripe phases, one has to admit that the predicted electronic properties show some difference to the experimental ones. In fact, our systematic studies of stripe phases completed within the relevant model for e_g orbitals, where several phases separated by different lattice spacing varying from $d = 3$ to $d = 11$ were considered, have revealed that the optimal stripe filling in the true ground state is slightly less ($0.86 \leq n_h \leq 0.89$ hole/Ni depending on the crystal field splitting) than the experimental value of one hole per Ni ion. This concerns the entire low doping regime, $x \leq 0.3$, where $\epsilon \simeq x$. There may be a few reasons of this discrepancy. First of all, one has to realize that in a multiband model with oxygen orbitals included explicitly the holes would be doped primarily to oxygen orbitals, screening the local moments at Ni sites,⁷⁴ in analogy to Zhang-Rice singlets in the cuprates.⁸³ An insulating ground state could then result from oxygen distortions by the Peierls mechanism. Thus, we argue that the present re-

TABLE III: Comparison of the free energy F (in the units of t) for the BC and SC stripe phases in the e_g model, and for BC stripe phases in the DDH model, obtained on 64×64 clusters at $x = 1/8$ hole doping. The free energy of the most stable phase (for BC or SC phases) is given in bold characters in each case. Parameters: $U = 8t$, $J_H = 1.5t$, $E_z = 0$, and $\beta t = 100$.

model	phase	diagonal stripes		vertical stripes	
		filled	half-filled	filled	half-filled
e_g	BC	2.5508	2.5759	2.5629	2.5756
	SC	2.7815	3.2615	2.7012	3.0729
DDH	BC	2.8172	2.8135	2.8395	2.8354

sults could be further improved within a realistic model including not only two e_g orbitals with different hopping elements, but also orbital polarization at oxygen sites. Second, it may be expected that the stripe filling will be somewhat changed due to the electron correlation effects beyond the HF approximation used here. We believe that the present work provides a good starting point for future studies of the correlation effects.

In summary we have analyzed the stripe formation in the doped nickelates in the realistic model with degeneracy of e_g orbitals, using large clusters. The results obtained with this model were compared with the widely used doubly degenerate Hubbard model. Even though in both models the distance between the DW is inversely proportional to the doping, the most stable diagonal stripes are found to differ markedly from one model to the other one. In the e_g model, the stripes are filled and nearly insulating, as observed experimentally in a series of layered nickelates. In contrast, in the DDH model they are half-filled and metallic. These latter stripe phases

are reminiscent of the stripes observed experimentally in largely doped cuprates. These differences have their roots in the different structure of intersite hopping terms. As the DDH model is closer to t_{2g} than to e_g hopping matrix elements, one might expect that doped insulators with t_{2g} orbital degrees of freedom, as in vanadates or in ruthenates, would promote different stripe phases than those observed in the nickelates.

Acknowledgments

We thank K. Rościszewski for insightful discussions. M.R. acknowledges support from the European Community under Marie Curie Program number HPMT2000-141. This work was supported by the Polish Ministry of Science and Education under Project No. 1 P03B 068 26, and by the Ministère Français des Affaires Étrangères under POLONIUM 09294VH.

-
- ¹ V. Sachan, D. J. Buttrey, J. M. Tranquada, J. E. Lorenzo, and G. Shirane, Phys. Rev. B **51**, 12742 (1995).
 - ² J. M. Tranquada, D. J. Buttrey, and V. Sachan, Phys. Rev. B **54**, 12318 (1996).
 - ³ S.-H. Lee and S.-W. Cheong, Phys. Rev. Lett. **79**, 2514 (1997).
 - ⁴ H. Yoshizawa, T. Kakeshita, R. Kajimoto, T. Tanabe, T. Katsufuji, and Y. Tokura, Phys. Rev. B **61**, R854 (2000).
 - ⁵ R. Kajimoto, T. Kakeshita, H. Yoshizawa, T. Tanabe, T. Katsufuji, and Y. Tokura, Phys. Rev. B **64**, 144432 (2001).
 - ⁶ S.-H. Lee, J. M. Tranquada, K. Yamada, D. J. Buttrey, Q. Li, and S.-W. Cheong, Phys. Rev. Lett. **88**, 126401 (2002).
 - ⁷ P. G. Freeman, A. T. Boothroyd, and D. Prabhakaran, D. González, and M. Enderle, Phys. Rev. B **66**, 212405 (2002).
 - ⁸ R. Kajimoto, K. Ishizaka, H. Yoshizawa, and Y. Tokura, Phys. Rev. B **67**, 014511 (2003).
 - ⁹ J. M. Tranquada, B. J. Sternlieb, J. D. Axe, Y. Nakamura, and S. Uchida, Nature **375**, 561 (1995).
 - ¹⁰ J. M. Tranquada, J. D. Axe, N. Ichikawa, Y. Nakamura, S. Uchida, and B. Nachumi, Phys. Rev. B **54**, 7489 (1996).
 - ¹¹ J. M. Tranquada, J. D. Axe, N. Ichikawa, A. R. Moodenbaugh, Y. Nakamura, and S. Uchida, Phys. Rev. Lett. **78**, 338 (1997).
 - ¹² N. Ichikawa, S. Uchida, J. M. Tranquada, T. Niemöller, P. M. Gehring, S.-H. Lee, and J. R. Schneider, Phys. Rev. Lett. **85**, 1738 (2000).
 - ¹³ P. M. Singer, A. W. Hunt, A. F. Cederström, and T. Imai, Phys. Rev. B **60**, 15345 (1999).
 - ¹⁴ S. Wakimoto, R. J. Birgeneau, Y. Fujimaki, N. Ichikawa, T. Kasuga, Y. J. Kim, K. M. Kojima, S.-H. Lee, H. Niko, J. M. Tranquada, S. Uchida, and M. von Zimmermann, Phys. Rev. B **67**, 184419 (2003).
 - ¹⁵ K. Yamada, C. H. Lee, K. Kurahashi, J. Wada, S. Wakimoto, S. Ueki, H. Kimura, Y. Endoh, S. Hosoya, G. Shirane, R. J. Birgeneau, M. Greven, M. A. Kastner, and Y. J. Kim, Phys. Rev. B **57**, 6165 (1998).
 - ¹⁶ E. Dagotto, *Nanoscale Phase Separation and Colossal Magnetoresistance*, Springer Series in Solid State Sciences Vol. 136 (Springer-Verlag, Heidelberg, 2003).
 - ¹⁷ T. Kimura, K. Hatsuda, Y. Ueno, R. Kajimoto, H. Mochizuki, H. Yoshizawa, T. Nagai, Y. Matsui, A. Yamazaki, and Y. Tokura, Phys. Rev. B **65**, 020407(R) (2002).
 - ¹⁸ S. Laroche, A. Mehta, L. Lu, P. K. Mang, O. P. Vajk, N. Kaneko, J. W. Lynn, L. Zhou, and M. Greven, Phys. Rev. B **71**, 024435 (2005).
 - ¹⁹ J. Zaanen and O. Gunnarsson, Phys. Rev. B **40**, 7391 (1989).
 - ²⁰ D. Poilblanc and T. M. Rice, Phys. Rev. B **39**, 9749 (1989).
 - ²¹ H. J. Schulz, J. Phys. (Paris) **50**, 2833 (1989); *ibid.* Phys. Rev. Lett. **64**, 1445 (1990).
 - ²² M. Kato, K. Machida, H. Nakanishi, and M. Fujita, J. Phys. Soc. Jpn. **59** 1047 (1990).
 - ²³ M. Inui and P. B. Littlewood, Phys. Rev. B **44**, 4415 (1991).
 - ²⁴ M. Raczkowski, A. M. Oleś, and R. Frésard, J. Low Temp. Phys., in press (2006); arXiv:cond-mat/0512420.
 - ²⁵ J. M. Tranquada, D. J. Buttrey, V. Sachan, and J. E. Lorenzo, Phys. Rev. Lett. **73**, 1003 (1994).
 - ²⁶ J. M. Tranquada, Y. Kong, J. E. Lorenzo, D. J. Buttrey, D. E. Rice, and V. Sachan, Phys. Rev. B **50**, 6340 (1994).
 - ²⁷ J. E. Lorenzo, J. M. Tranquada, D. J. Buttrey, and V. Sachan, Phys. Rev. B **51**, 3176 (1995).
 - ²⁸ J. M. Tranquada, J. E. Lorenzo, D. J. Buttrey, and V. Sachan, Phys. Rev. B **52**, 3581 (1995).
 - ²⁹ J. M. Tranquada, P. Wochner, A. R. Moodenbaugh, and D. J. Buttrey, Phys. Rev. B **55**, R6113 (1997).
 - ³⁰ J. M. Tranquada, P. Wochner, and D. J. Buttrey, Phys. Rev. Lett. **79**, 2133 (1997).
 - ³¹ P. Wochner, J. M. Tranquada, D. J. Buttrey, and V. Sachan, Phys. Rev. B **57**, 1066 (1998).
 - ³² K. Ishizaka, Y. Taguchi, R. Kajimoto, H. Yoshizawa, and Y. Tokura, Phys. Rev. B **67**, 184418 (2003).

- ³³ C. H. Chen, S-W. Cheong, and A. S. Cooper, Phys. Rev. Lett. **71**, 2461 (1993).
- ³⁴ E. D. Isaacs, G. Aeppli, P. Zschack, S-W. Cheong, H. Williams, and D. J. Buttrey, Phys. Rev. Lett. **72**, 3421 (1994).
- ³⁵ A. Vigliante, M. von Zimmermann, J. R. Schneider, T. Frello, N. H. Andersen, J. Madsen, D. J. Buttrey, D. Gibbs, and J. M. Tranquada, Phys. Rev. B **56**, 8248 (1997).
- ³⁶ K. Ishizaka, T. Arima, Y. Murakami, R. Kajimoto, H. Yoshizawa, N. Nagaosa, and Y. Tokura, Phys. Rev. Lett. **92**, 196404 (2004).
- ³⁷ J. Li, Y. Zhu, J. M. Tranquada, K. Yamada, and D. J. Buttrey, Phys. Rev. B **67**, 012404 (2003).
- ³⁸ The Q_c and Q_s values correspond to (ϵ, ϵ) and to $(1/2 \pm \epsilon/2, 1/2 \pm \epsilon/2)$ in the notation used in experimental papers.
- ³⁹ J. H. Jung, D.-W. Kim, T. W. Noh, H. C. Kim, H.-C. Ri, S. J. Levett, M. R. Lees, D. McK. Paul, and G. Balakrishnan, Phys. Rev. B **64**, 165106 (2001).
- ⁴⁰ K. Yamamoto, K. Ishizaka, E. Saitoh, S. Shinomori, T. Tanabe, T. Katsufuji, and Y. Tokura, Phys. Rev. B **67**, 014414 (2003).
- ⁴¹ N. Poirot-Reveau, Ph. Odier, P. Simon, and F. Gervais, Phys. Rev. B **65**, 094503 (2002).
- ⁴² A. P. Ramirez, P. L. Gammel, S-W. Cheong, D. J. Bishop, and P. Chandra, Phys. Rev. Lett. **76**, 447 (1996).
- ⁴³ S-W. Cheong, H. Y. Hwang, C. H. Chen, B. Batlogg, L. W. Rupp, Jr., and S. A. Carter, Phys. Rev. B **49**, 7088 (1994).
- ⁴⁴ T. Katsufuji, T. Tanabe, T. Ishikawa, Y. Fukuda, T. Arima, and Y. Tokura, Phys. Rev. B **54**, R14230 (1996).
- ⁴⁵ T. Katsufuji, T. Tanabe, T. Ishikawa, S. Yamanouchi, Y. Tokura, T. Kakeshita, R. Kajimoto, and H. Yoshizawa, Phys. Rev. B **60**, R5097 (1999).
- ⁴⁶ M. Satake, K. Kobayashi, T. Mizokawa, A. Fujimori, T. Tanabe, T. Katsufuji, and Y. Tokura, Phys. Rev. B **61**, 15515 (2000).
- ⁴⁷ S. R. White and D. J. Scalapino, Phys. Rev. Lett. **80**, 1272 (1998).
- ⁴⁸ S. R. White and D. J. Scalapino, Phys. Rev. B **60**, R753 (1999).
- ⁴⁹ G. Seibold, E. Sigmund, and V. Hizhnyakov, Phys. Rev. B **57**, 6937 (1998).
- ⁵⁰ G. Seibold, C. Castellani, C. Di Castro, and M. Grilli, Phys. Rev. B **58**, 13506 (1998).
- ⁵¹ G. Seibold and J. Lorenzana, Phys. Rev. B **69**, 134513 (2004).
- ⁵² D. Góra, K. Rościszewski, and A. M. Oleś, Phys. Rev. B **60**, 7429 (1999).
- ⁵³ T. Tohyama, S. Nagai, Y. Shibata, and S. Maekawa, Phys. Rev. Lett. **82**, 4910 (1999).
- ⁵⁴ P. Wróbel and R. Eder, Phys. Rev. B **62**, 4048 (2000).
- ⁵⁵ P. Wróbel, A. Maciąg, and R. Eder, J. Phys.: Condens. Matter **18**, 1249 (2006); arXiv:cond-mat/0408703 (unpublished).
- ⁵⁶ M. Fleck, A. I. Lichtenstein, E. Pavarini, and A. M. Oleś, Phys. Rev. Lett. **84**, 4962 (2000); M. Fleck, A. I. Lichtenstein, and A. M. Oleś, Phys. Rev. B **64**, 134528 (2001).
- ⁵⁷ M. G. Zacher, R. Eder, E. Arrigoni, and W. Hanke, Phys. Rev. Lett. **85**, 2585 (2000); Phys. Rev. B **65**, 045109 (2002).
- ⁵⁸ F. Becca, L. Capriotti, and S. Sorella, Phys. Rev. Lett. **87**, 167005 (2001).
- ⁵⁹ J. A. Riera, Phys. Rev. B **64**, 104520 (2001).
- ⁶⁰ J. Zaanen and P. B. Littlewood, Phys. Rev. B **50**, 7222 (1994).
- ⁶¹ T. Mizokawa and A. Fujimori, Phys. Rev. B **56**, 11920 (1997).
- ⁶² Ya-Sha Yi, Zhi-Gang Yu, A. R. Bishop, and J. T. Gammel, Phys. Rev. B **58**, 503 (1998); R. J. McQueeney, A. R. Bishop, Ya-Sha Yi, and Z. G. Yu, J. Phys.: Condens. Matter **12**, 317 (2000).
- ⁶³ T. Hotta and E. Dagotto, Phys. Rev. Lett. **92**, 227201 (2004).
- ⁶⁴ A. M. Oleś and J. Zaanen, Phys. Rev. B **39**, 9175 (1989).
- ⁶⁵ J. D. Jorgensen, B. Dabrowski, Shiyong Pei, D. R. Richards, and D. G. Hinks, Phys. Rev. B **40**, 2187 (1989).
- ⁶⁶ P. G. Radaelli, D. G. Hinks, A. W. Mitchell, B. A. Hunter, J. L. Wagner, B. Dabrowski, K. G. Vandervoort, H. K. Viswanathan, and J. D. Jorgensen, Phys. Rev. B **49**, 4163 (1994).
- ⁶⁷ R. Frésard, M. Raczowski, and A. M. Oleś, Phys. Stat. Sol. (b) **242**, 370 (2005).
- ⁶⁸ A. Takahashi and H. Shiba, Eur. Phys. J. B **5**, 413 (1998).
- ⁶⁹ The electronic structure in the three-dimensional case was recently analyzed in Ref. 82.
- ⁷⁰ P. Kuiper, J. van Elp, G. A. Sawatzky, A. Fujimori, S. Hosoya, and D. M. de Leeuw, Phys. Rev. B **44**, 4570 (1991).
- ⁷¹ H. Eisaki, S. Uchida, T. Mizokawa, H. Namatame, A. Fujimori, J. van Elp, P. Kuiper, G. A. Sawatzky, S. Hosoya, and H. Katayama-Yoshida, Phys. Rev. B **45**, 12513 (1992).
- ⁷² J. Bała, A. M. Oleś, and J. Zaanen, Phys. Rev. B **61**, 13573 (2000).
- ⁷³ J. B. Grant and A. K. McMahan, Phys. Rev. B **46**, 8440 (1992).
- ⁷⁴ J. Zaanen and G. A. Sawatzky, J. Solid State Chem. **88**, 8 (1990).
- ⁷⁵ A. M. Oleś, G. Khaliullin, P. Horsch, and L. F. Feiner, Phys. Rev. B **72**, 214431 (2005).
- ⁷⁶ J. S. Griffith, *The Theory of Transition Metal Ions* (Cambridge University Press, Cambridge, 1971).
- ⁷⁷ A. E. Bocquet, T. Mizokawa, T. Saitoh, H. Namatame, and A. Fujimori, Phys. Rev. B **46**, 3771 (1992).
- ⁷⁸ P. Mahadevan, K. Sheshadri, D. D. Sarma, H. R. Krishnamurthy, and R. Pandit, Phys. Rev. B **55**, 9203 (1997).
- ⁷⁹ J. B. Grant and A. K. McMahan, Physica C **162**, 1439 (1989).
- ⁸⁰ P. Kuiper, J. van Elp, D. E. Rice, D. J. Buttrey, H.-J. Lin, and C. T. Chen, Phys. Rev. B **57**, 1552 (1998).
- ⁸¹ A. M. Oleś, Phys. Rev. B **28**, 327 (1983); A. Klejnberg and J. Spalek, *ibid.* **57**, 12041 (1998); **61**, 15542 (2000).
- ⁸² L. F. Feiner and A. M. Oleś, Phys. Rev. B **71**, 144422 (2005).
- ⁸³ F. C. Zhang and T. M. Rice, Phys. Rev. B **37**, 3759 (1988).